PI Parameter Tuning of Converters for Sub-Synchronous Interactions Existing in Grid-connected DFIG Wind Turbines

Aikang Chen[1], Da Xie[1*], *Member, IEEE*, Daming Zhang[2], *Member, IEEE*, Chenghong Gu[3], *Member, IEEE*, Keyou Wang[1], *Member, IEEE*

[1] Department of Electrical Engineering, Shanghai Jiao Tong University, Shanghai, China; e-mails: 381315687@sjtu.edu.cn (A. Chen); wangkeyou@sjtu.edu.cn (K. Wang)

[2] School of Electrical Engineering and Telecommunication, UNSW, Australia; e-mail: daming.zhang@unsw.edu.au

[3] Department of Electronic and Electrical Engineering, University of Bath, Bath, U.K; e-mail: C.Gu@bath.ac.uk

***** Correspondence: profxzgl@hotmail.com; Tel.: +86-156-1866-9531

***Abstract*—Wind power is essential worldwide to supply clean energy, but oscillations in wind turbine generators could severely affect the stability of power systems, particularly those from controllers. This paper employs the small-signal model to investigate the influence of converters' PI parameters tuning on sub-synchronous interactions (SSI) in a grid-connected doubly fed induction generator (DFIG). With eigenvalue and participation factors analysis, oscillation modes that mainly determined by PI parameters are clarified. A novel optimization model with the reference-point based Non-Dominated Sorting Genetic Algorithm (NSGA-III) and the t-distributed stochastic neighbour embedding (t-SNE) is developed to explore and visually analyze the optimal PI parameters ranges. This can facilitate the selection of the appropriate PI parameters to augment the damping ratios of corresponding oscillation modes. Additionally, in order to study the adaptability of the optimal PI parameters, interactions performance of the system that uses these parameters is studied with different output levels of the wind turbine generator. Finally, a time domain simulation and a practical experiment are conducted to demonstrate the correctness of the proposed approach. Results illustrate that the SSI of a grid-connected DFIG is suppressed with the optimization model. This study is highly beneficial to power system operators in integrating wind power and maintaining system stability.**

***Index Terms*—Converters, optimization methods, power system stability, wind power generation**

I. INTRODUCTION

The utilization of wind power is rapidly increasing worldwide as one of the most promising renewable power sources [1,2]. Among several wind generation technologies, variable speed wind turbines utilizing doubly fed induction generators (DFIGs) have attracted special attention because of their advantages over other types of wind turbines [3, 4]. In addition, more wind farms are expected to connect to power systems through series-compensated lines, which may produce adverse effects with other power

system components, such as sub-synchronous interaction [5]. There are several types of SSI, including sub-synchronous oscillation (SSO), sub-synchronous resonance (SSR), and sub-synchronous control interaction (SSCI) [6-8].

Mechanical oscillations are critical since they induce fatigue stresses on drive-train components, increasing the risk of damage to the mechanical systems. For instance, torsional vibrations in a wind turbine shaft, which can be excited by turbulent winds or grid faults and disturbances, can result in significant stresses and fatigue on gearboxes. Since a single-mass shaft model cannot properly represent mechanical oscillations, wind turbines are described with at least a two-mass [9] or three-mass models [10] to investigate torsional oscillation frequencies. SSO is an electric power system condition where the network exchanges significant energy with a turbine generator at one or more natural frequencies lower than the system synchronous frequency [11]. Therefore, the torsional oscillations belong to SSO. The torsional oscillations can be mechanically damped by pitch control, mechanical dampers in wind turbine drive-train, or external devices such as flexible alternating current transmission system (FACTS) [12-14].

SSR is a condition where a series capacitor compensated system exchanges significant energy with a turbine-generator at a frequency below the synchronous frequency [15]. For wind farms connected to series-compensated lines, the energy exchange and interactions between mechanical and electrical system are expected to cause SSR with a resonant frequency below the fundamental frequency [16]. SSR in wind farms has been studied in recent literature [17, 18]. The mitigation of SSR using FACTS devices, such as TCSC and SVC, has been explored in wind farms connected with series compensated transmission networks [19, 20].

SSCI is an interaction between a power electronic control system and a series-compensated electrical network [21]. Due to that, an SSCI occurred at a wind farm in Texas, NERC has issued a Lesson Learned document for the SSI between series compensated transmission lines and wind generation [22, 23]. In [24] a two-step approach, comprising of a frequency-domain impedance scan screening and a time-domain simulation, is proposed to verify the presence of SSCI by using the IEEE Second Benchmark Model. To mitigate SSCI, [25] presents an overview of SSCI and designs a SSCI damping controller in PSCAD using a Type 3 wind turbine model.

Eigenvalue analysis based on the small-signal model is a well-developed approach to identify the oscillation frequencies [29,30]. To study the stability of a permanent magnet synchronous generator based wind turbine, the impact of controllers' parameters on the traces of eigenvalues is analyzed to design controllers' parameters [31]. The impact of a damping controller on different operation modes for DFIG-based wind generation systems is investigated in [32]. However, the damping of SSI of the DFIG-based wind turbine by changing converters' PI parameters have seldom been investigated.

Currently, PI control is the pivotal and fundamental controller in the control strategies of converters for grid-connected DFIG wind turbines, with its reliability, efficiency, and convenience in engineering. The variations of PI parameters are closely related to system vibration performance, especially SSI. In Yancheng, China, destructive SSI was captured in wind farms, causing severe damage of crowbar circuits and gearboxes, due to the interaction between the control of converters and fixed series compensation

in DFIG [33]. Recently, compensation methods have engaged the attention of existing research, especially supplementary control and compensation devices. Authors of [34, 35] added auxiliary control in control loops of converters to enhance the stable region and to damp the vibrations, which, however, increased the complexity of systems and the difficulty of stability analysis. The use of flexible AC transmission systems (FACTS), such as STATCOM and series capacitor is proposed in [36, 37]. The main drawback of this method is the cost of the device and its protection equipment. Hence, engineers incline to PI tuning for SSI suppression. Whereas multiple PI parameter tuning involves system coupling problem, single PI parameters and the set of PI parameters they constitute make a different influence on SSI modes [38], leading PI tuning has been a tremendous difficulty in engineering. Exiting engineering PI tuning method lacks enough theoretical support and is unsystematic.

This paper combines the small-signal model and eigenvalue analysis to transform vibration abatement into PI parameter tuning. Then NSGA-3 is employed for optimization with more than two objectives in case of local optimization. Additionally, the results of multi-objective optimization are apt to be too broad to achieve better SSI suppression. A processing method based on t-SNE, a dimensional reduction method, is developed to address the issue, removing the undesirable results by intuitional comparison of final results and in-process results under two-dimensional space. Finally, the optimal results from the developed model are validated from three aspects: by analyzing the traces of eigenvalues with the different generated power to study the adaptability of the PI parameters, by implementing a time domain simulation on MATLAB/Simulink, and by conducting a practical experiment on the system.

The major contributions of this paper are threefold:

- It connects PI parameter tuning of converters with SSI mitigation, and constructs an optimization model based on NSGA-3 for grid-connected DFIGs, increasing the damping of SSI for vibration suppression.
- Optimal PI parameter range is extracted from broad optimization results with a dimension reduction technique based on t-SNE.
- PI parameter tuning in the single machine can improve the stabilization and extend the lifespan of a single machine, and therefore, enlarge the stable region of the wind farm.

The rest of the paper is organized as follows: Section II introduces the small-signal model of each part and the whole system. Oscillation modes analysis of the small-signal is conducted in section III. Section IV constructs an optimization model with NSGA-III and t-SNE to investigate the impact of converters' PI parameters on the traces of eigenvalues and find the optimal PI parameters. Section V combines the universality analysis, time domain simulation and practical experiment to verify the accuracy of the optimal PI parameters. Conclusions are drawn in Section VI.

II. SMALL-SIGNAL MODELLING OF THE DFIG

The schematic diagram of the studied system is presented in Fig. 1, where the DFIG wind turbine is connected to an infinite bus system through a transmission line. The system consists of a three-mass shaft, an induction generator, a rotor side converter (RSC), a grid side converter (GSC), a GSC side reactance, and a transmission line. Subsequently, this paper gives a brief introduction to the small-signal model, and its detailed modelling process can be referred to [29].

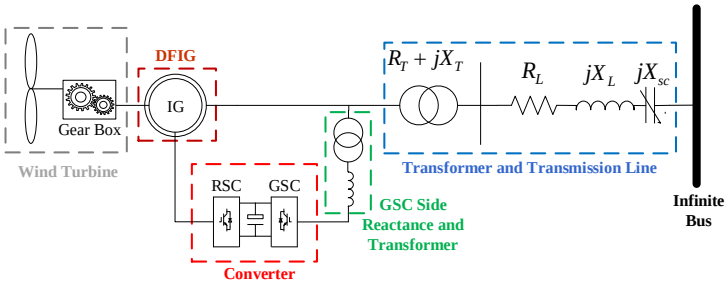

Fig. 1 Block diagram of the DFIG-based wind generator model

A. *Model of Three-mass Shaft and Induction Generator*

The wind turbine drive train generally comprises a windmill blade, a low-speed shaft, a gearbox, a high-speed shaft and a generator rotor, and a three-mass model is therefore employed in this study. Within the three-mass model, the inertia of the gearbox is shared between the low-speed shaft and high-speed shaft, and the inertia of the high-speed shaft aggregates the inertia of the generator. Thus, all three masses are corresponding to the mass moment of the inertia of blades, low-speed shaft, and high-speed shaft, respectively [39, 40].

For modelling the induction generator model, machine equations are represented in the synchronously rotating frame where the direction of d-axis is aligned with the rotor's magnetic flux linkage.

B. *Model of RSC*

The rotor side converter aims to control the output active power to track the input of the wind turbine torque. The decoupled control strategy is used for the DFIG system to regulate its output power, as shown in Fig. 2.

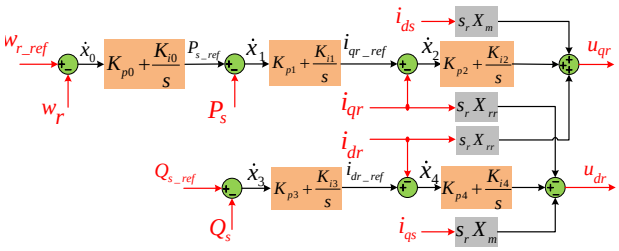

Fig. 2 Control block diagram of the rotor side converter

By introducing variables x_0, x_1, x_2, x_3 and x_4, the rotor side converter model can be expressed by (4).

$$\begin{cases} \Delta P_s = i_{ds0}\Delta u_{ds} + u_{ds0}\Delta i_{ds} + i_{qs0}\Delta u_{qs} + u_{qs0}\Delta i_{qs} \\ \Delta Q_s = i_{ds0}\Delta u_{qs} + u_{qs0}\Delta i_{ds} - i_{qs0}\Delta u_{ds} - u_{ds0}\Delta i_{qs} \\ \Delta \dot{x}_0 = \Delta \omega_{r\_ref} - \Delta \omega_r \\ \Delta \dot{x}_1 = \Delta P_{s\_ref} - \Delta P_s \\ \Delta \dot{x}_2 = K_{p1}\left(\Delta P_{s\_ref} - \Delta P_s\right) + K_{i1}\Delta x_1 - \Delta i_{qr} \\ \Delta \dot{x}_3 = \Delta Q_{s\_ref} - \Delta Q_s \\ \Delta \dot{x}_4 = K_{p3}\left(\Delta Q_{s\_ref} - \Delta Q_s\right) + K_{i3}\Delta x_3 - \Delta i_{dr} \end{cases} \tag{1}$$

where u_{ds} and u_{qs} are the d and q axis stator voltages, i_{ds} and i_{qs} are the d and q axis stator currents, ω_r is the high-speed shaft angle speed which is equal to the generator angle speed, i_{dr} and i_{qr} are the d and q axis rotor currents.

The output variables of the grid side converter are given by

$$\begin{cases} \Delta u_{dr} = K_{p4}\Delta \dot{x}_4 + K_{i4}\Delta x_4 - X_m i_{qs0}\Delta s \\ \qquad - X_m s_{r0}\Delta i_{qs} - X_{rr} i_{qr0}\Delta s_r - X_{rr} s_{r0}\Delta i_{qr} \\ \Delta u_{qr} = K_{p2}\Delta \dot{x}_2 + K_{i2}\Delta x_2 + X_m i_{ds0}\Delta s_r \\ \qquad + X_m s_{r0}\Delta i_{ds} + X_{rr} i_{dr0}\Delta s_r + X_{rr} s_{r0}\Delta i_{dr} \end{cases} \tag{2}$$

Where X_m is the mutual inductive reactance, $u_{dr,}$ and u_{qr} are d and q axis rotor voltages.

C. Model of GSC

The dc-link voltage is maintained by controlling the grid-side converter using the decoupled d-q vector control, with the d-q frame oriented along the stator voltage vector position. As shown in Fig. 3, the dc-link is controlled by i_{dg} while the reactive power is controlled by i_{qg}.

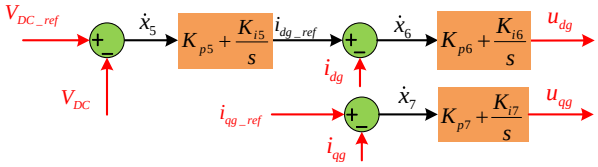

Fig. 3 Control block diagram of the grid side converter

With introducing variables x_5, x_6 and x_7, the grid side converter model can be expressed by the following equations

$$\begin{cases} \Delta \dot{x}_5 = \Delta V_{DC\_ref} - \Delta V_{DC} \\ \Delta \dot{x}_6 = K_{p5}\left(\Delta V_{DC\_ref} - \Delta V_{DC}\right) + K_{i5}\Delta x_5 - \Delta i_{dg} \\ \Delta \dot{x}_7 = \Delta i_{qg\_ref} - \Delta i_{qg} \end{cases} \tag{3}$$

Where V_{DC} is the dc-link voltage, defining its positive direction as discharging direction.

The output variables of the grid side converter are given by

$$\begin{cases} \Delta u_{dg} = K_{p6}\Delta\dot{x}_6 + K_{i6}\Delta x_6 \\ \Delta u_{qg} = K_{p7}\left(\Delta i_{qg\_ref} - \Delta i_{qg}\right) + K_{i7}\Delta x_7 \end{cases} \tag{4}$$

D. Model of DC-link, Grounded Capacitor, GSC side Reactance and Transformer, and Transmission Line

The dc-link model can be obtained according to that the active power flow through the converters is balanced. And the differential equations of the grounded capacitor can be derived from the relationship between the capacitor voltage and current. In terms of the GSC side reactance and transformer and the transmission line, they are equal to an RL line and an RLC line.

E. Model of the Whole System

To study the system stability after suffering a small disturbance, it is necessary to build the complete small-signal model of the system, as shown in Fig. 4.

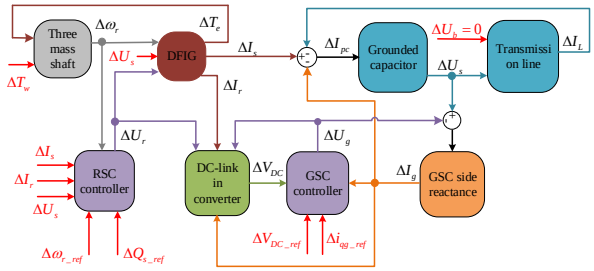

Fig. 4 Small-signal model of DFIG to an infinite bus

By solving the Equations above, the union model can be written in a compact form in

$$\Delta\dot{X} = A\Delta X + B\Delta u \tag{5}$$

$$\begin{aligned} \Delta X =& \left[\Delta X_M, \Delta X_G, \Delta X_{RSR}, \Delta X_{DC}, \Delta X_{GSI}, \Delta X_{RL}, \Delta X_{PC}, \Delta X_{TL}\right]^T \\ =& \left[\Delta\theta_{turb}, \Delta\theta_{gear}, \Delta\theta_r, \Delta\omega_{turb}, \Delta\omega_{gear}, \Delta\omega_r, \right. \\ & \Delta\psi_{qs}, \Delta\psi_{ds}, \Delta\psi_{qr}, \Delta\psi_{dr}, \ \Delta x_0, \Delta x_1, \Delta x_2, \Delta x_3, \Delta x_4 \\ & \Delta V_{DC}, \ \Delta x_5, \Delta x_6, \Delta x_7, \ \Delta i_{gx}, \Delta i_{gy}, \ \Delta u_{gc,x}, \Delta u_{gc,y} \\ & \left. \Delta i_{Lx}, \Delta i_{Ly}, \Delta u_{sc,x}, \Delta u_{sc,y}\right]^T \end{aligned} \tag{6}$$

$$\Delta u = \left[\Delta T_w \ \ \Delta\omega_{r\_ref} \ \ \Delta Q_{s\_ref} \ \ \Delta V_{DC\_ref} \ \ \Delta i_{qg\_ref} \ \ \Delta U_b\right]^T \tag{7}$$

Where θ_{turb}, θ_{gear}, θ_r are respectively the twist angles of the wind turbine, low-speed shaft and high-speed shaft, ω_{turb} is the wind turbine angle speed, ω_{gear} is the low-speed shaft angle speed, ψ_{ds} and ψ_{qs} are the d and q axis stator flux, ψ_{dr} and ψ_{qr} are the d and q axis rotor flux, i_{gx} and i_{gy} are the x and y axis currents, $u_{gc,x}$ and $u_{gc,y}$ are the x and y axis voltages, $u_{sc,x}$ and $u_{sc,y}$ are the x and y axis voltages; i_{Lx} and i_{Ly} are the x and y axis currents.

III. Oscillation Mode Analysis with the Small-signal Model

TABLE I Parameters of PI Controllers

Parameter	Value	Parameter	Value
K_{p0}	300	K_{i0}	1100
K_{p1}	0.05	K_{i1}	0.0004
K_{p2}	5	K_{i2}	6
K_{p3}	0.5	K_{i3}	0.0002
K_{p4}	5	K_{i4}	5
K_{p5}	1.5	K_{i5}	65
K_{p6}	0.93	K_{i6}	0.05
K_{p7}	0.83	K_{i7}	20

The small signal model of the above system is built in MATLAB/Simulink. The PI parameters applied in practical engineering are shown in Table I. The eigenvalues of the system is shown in Table II. It can be seen that the system is stable after suffering a small disturbance because all the eigenvalues have negative real parts. There are nine oscillation modes and nine evanescent modes. The participation factors can disclose the relationship between the modes and variables, as shown in Table III, and the values in the table need to be multiplied by 10^{-4}.

TABLE II Eigenvalues of the Small Signal System

No.	Eigenvalues	Oscillation frequency, Hz	Damping
$\lambda_{1,2}$	$-1715.5\pm2.68\times10^{8}$i	4.26×10^{7}	0
$\lambda_{3,4}$	$-3189.3\pm1.35\times10^{8}$i	2.15×10^{7}	0
λ_{5}	-942.2	0	1
$\lambda_{6,7}$	-23.63±498i	79.25	0.0474
$\lambda_{8,9}$	-51.17±285i	45.37	0.1767
$\lambda_{10,11}$	-16.75±147i	23.40	0.1132
λ_{12}	-139.8	0	1
$\lambda_{13,14}$	-1.477±77.97i	12.41	0.0189
$\lambda_{15,16}$	-8.91±27.45i	4.37	0.3087
$\lambda_{17,18}$	-11.72±12.08i	1.92	0.6963
$\lambda_{19,20}$	-0.319±3.177i	0.51	0.1
λ_{21}	-2.74	0	1
λ_{22}	-1.20	0	1
λ_{23}	-1.00	0	1
λ_{24}	-0.0538	0	1
λ_{25}	-0.008	0	1
λ_{26}	-0.0003	0	1
λ_{27}	-1.825×10^{-14}	0	1

TABLE III Participation Factors of State Variables

	$\lambda_{1,2}$	$\lambda_{3,4}$	$\lambda_{6,7}$	$\lambda_{8,9}$	$\lambda_{10,11}$	$\lambda_{13,14}$	$\lambda_{15,16}$	$\lambda_{17,18}$	$\lambda_{19,20}$
Δi_{Lx}	0	106	**2106**	6	**1545**	30	49	80	4
Δi_{Ly}	34	0	**2415**	5	**1307**	20	85	52	3
$\Delta u_{sc,x}$	0	0	**2521**	39	**1870**	14	39	23	1
$\Delta u_{sc,y}$	0	0	**2605**	42	**2030**	18	23	31	2
$\Delta u_{gc,x}$	0	**3944**	0	0	0	0	0	0	0
$\Delta u_{gc,y}$	**5000**	0	0	0	0	0	0	0	0
$\Delta \psi_{qs}$	**1529**	0	175	**1363**	711	22	72	108	7
$\Delta \psi_{ds}$	0	**4758**	385	**1282**	370	12	12	49	2
$\Delta \psi_{qr}$	**3393**	0	32	120	260	13	59	107	5
$\Delta \psi_{dr}$	0	**1056**	160	319	335	14	38	85	4

$\Delta\theta_1$	0	0	0	0	0	2	4	102	**1734**
$\Delta\theta_2$	0	0	0	0	4	**4499**	150	429	15
$\Delta\theta_3$	0	0	0	0	13	564	99	**1594**	864
$\Delta\omega_1$	0	0	0	0	0	2	4	102	**1734**
$\Delta\omega_2$	0	0	0	0	4	**4499**	151	433	15
$\Delta\omega_r$	0	0	10	67	302	575	995	**3659**	70
Δx_3	0	0	0	0	0	0	0	0	0
Δx_4	0	0	0	0	2	7	3	38	27
Δx_5	0	0	0	65	50	7	**3554**	695	3
Δx_6	0	0	0	0	0	0	7	2	0
ΔV_{DC}	0	0	4	427	172	15	**7167**	543	**2082**
Δi_{gx}	0	136	102	**2957**	351	8	34	43	1
Δi_{gy}	44	0	42	**3266**	424	5	808	158	3
Δx_7	0	0	0	37	19	1	962	549	337
Δx_0	0	0	0	0	7	8	265	**1112**	740
Δx_1	0	0	0	0	0	0	1	2	3
Δx_2	0	0	0	2	3	0	7	5	4

According to the eigenvalues in Table II and the participation factors in Table III, the oscillation modes can be classified into electrical resonance, SSR, SSO, SSCI, and low-frequency oscillation. Classification of these interactions in a DFIG-based generation system is shown in Fig. 5.

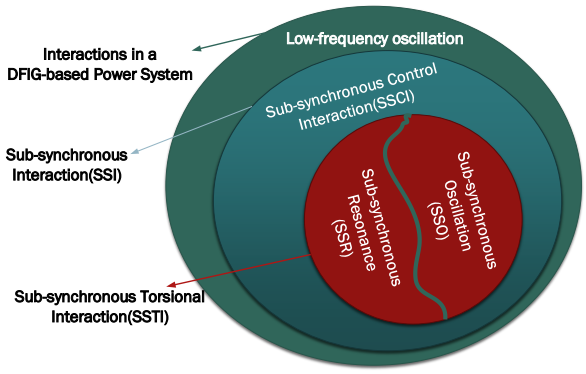

Fig. 5 Classification of interactions in a DFIG-based generation system

The specific analysis is as follows:

i) Electrical Resonance

As shown in Table III, $\lambda_{1,2}$ are highly sensitive to $\Delta u_{gc,y}$, $\Delta\psi_{qs}$ and $\Delta\psi_{qr}$, and $\lambda_{3,4}$ are highly sensitive to $\Delta u_{gc,x}$, $\Delta\psi_{ds}$ and $\Delta\psi_{dr}$, so they are mainly affected by the generator and grounded capacitor. Therefore, they belong to electrical resonance. The corresponding oscillation frequencies of $\lambda_{1,2}$ and $\lambda_{3,4}$ are very high due to the small value of the grounded capacitance. Generally, the grounded capacitor is equal to the open circuit and has no effect on the whole system. Therefore, the two oscillation modes are not the emphasis of the system.

$\lambda_{8,9}$ are highly sensitive to $\Delta\psi_{qs}$, $\Delta\psi_{ds}$, Δi_{gx} and Δi_{gy}, so they are mainly affected by the generator and the GSC side reactance. Therefore, they also belong to the category of electrical resonance.

ii) Sub-Synchronous Resonance

In a series-compensated power system, the resonance frequency is influenced by compensation level $k_{com}=X_{sc}/X_L$, where X_{sc} is the reactance of the series capacitor, and X_L is the total reactance of the transmission line, transformers, and generator. In the small signal model simulation, the compensation level is 35%. Therefore, the system resonance frequency is given by

$$f_e = f_0\sqrt{k_{com}} = 50\times\sqrt{0.35} = 29.58\text{Hz} \tag{8}$$

where f_0 is the synchronous frequency.

In the system, $\lambda_{6,7}$ and $\lambda_{10,11}$ are highly sensitive to Δi_{Lx}, Δi_{Ly}, $\Delta u_{sc,x}$ and $\Delta u_{sc,y}$, so they are mainly affected by the transmission line and the series capacitor. Moreover, the oscillation frequency of $\lambda_{6,7}$ is 79.25Hz, which is approximately equal to $50+f_e$=79.58Hz. The oscillation frequency of $\lambda_{10,11}$ is 23.40Hz, which is approximately equal to $50-f_e$=20.42Hz.

Therefore, the oscillation mode of $\lambda_{6,7}$ belongs to the category of super-synchronous resonance and that of $\lambda_{10,11}$ belongs to the category of sub-synchronous resonance.

iii) Sub-Synchronous Oscillation

$\lambda_{13,14}$ are highly sensitive to $\Delta\theta_2$ and $\Delta\omega_2$, and slightly sensitive to $\Delta\theta_3$ and $\Delta\omega_r$, so they are mainly affected by the three mass shafts. $\lambda_{17,18}$ are highly sensitive to $\Delta\theta_3$, $\Delta\omega_r$, $\Delta\theta_2$, and $\Delta\omega_2$, and also sensitive to ΔV_{DC}, Δx_0, Δx_5, and Δx_7, so they are mainly affected by the three mass shafts and the converter controller. Therefore, the oscillation modes of $\lambda_{13,14}$ and $\lambda_{17,18}$ belong to the category of SSO. $\lambda_{13,14}$ is corresponding to the low-speed shaft, while $\lambda_{17,18}$ is corresponding to the high-speed shaft.

iv) Sub-Synchronous Control Interaction

The SSCI is not related to the mechanical shaft system and may change under different system conditions and converter control algorithms. In the system, $\lambda_{15,16}$ are highly sensitive to Δx_5 and ΔV_{DC}, and also sensitive to $\Delta\omega_r$, so they are mainly affected by the converter controller and rotor speed of the generator. Therefore, the oscillation mode of $\lambda_{15,16}$ belongs to the category of SSCI.

v) Low-Frequency Oscillation

In the system, $\lambda_{19,20}$ are highly sensitive to $\Delta\theta_1$, $\Delta\theta_r$, $\Delta\omega_1$, and Δx_0, so they are mainly affected by the three mass shafts and rotor speed control of the generator. Therefore, the oscillation mode of $\lambda_{19,20}$ belongs to the category of low-frequency oscillation.

According to the oscillation modes analysis above, it is found that the interactions of the grid-connected DFIG system change with PI parameters of converters, manifested in eigenvalues variations of the system. In particular, oscillation modes of $\lambda_{15,16}$ and $\lambda_{17,18}$ have a strong association with PI parameters, and $\lambda_{8,9}$, $\lambda_{10,11}$, $\lambda_{13,14}$ and $\lambda_{19,20}$ are also affected by PI parameters.

IV. Optimization Model of Sub-Synchronous Interactions

Practical PI parameters listed in Table I can keep DFIG system stable, but this set of PI parameters is far from optimal. To strengthen the dynamic performance of the system, there remains a need for an efficient method that can choose applicable

controllers' PI parameters to increase the damping ratios of oscillation modes. In addition, to visualize the optimization results for a better understanding of the relation between PI parameters and the oscillation modes, a dimension reduction algorithm is essential.

This section introduces a multiobjective optimization model, which is applied to the grid-connected DFIG system and based on NSGA-III and t-SNE, to maximize the damping ratios of $\lambda_{8,9}$, $\lambda_{10,11}$, $\lambda_{13,14}$, $\lambda_{15,16}$, $\lambda_{17,18}$, and $\lambda_{19,20}$. In general, every two eigenvalues are conjugated, which means that the number of damping ratios is six. However, twelve objects are considered for the universality and their fitness functions can be expressed as

$$f_i = \frac{\mathrm{Re}(\lambda_i)}{\sqrt{\mathrm{Re}(\lambda_i)^2 + \mathrm{Im}(\lambda_i)^2}} \quad i = 8,9,10,11,13,14,15,16,17,18,19,20 \tag{9}$$

Based on the eigenvalue analysis method, the real part of the eigenvalue must be negative to ensure the stability. Moreover, the ranges of values allowed for PI parameters are 1/10 to 10 times of the set values in section II in order to facilitate the computing. Hence, the objective function of the optimization model and its constraints are

$$\begin{aligned} &Obj = \max\left[f_{8,9}, f_{12}, f_{13,14}, f_{15,16}, f_{17,18}, f_{19,20}, f_{21} \right] \\ &s.t. \\ &\quad \mathrm{Re}(\lambda_i) < 0,\ \mathrm{i}=8,9,10,11,13,14,15,16,17,18,19,20 \\ &\quad 0.1K_{pm} \le K_{pm} \le 10K_{pm}, m = 0,1,\cdots 7 \\ &\quad 0.1K_{im} \le K_{im} \le 10K_{im}, m = 0,1,\cdots 7 \end{aligned} \tag{10}$$

A. The Procedure of NSGA-III

NSGA-III is an efficient evolutionary algorithm for multiobjective optimization, and its core concept is combining the dominance criterion and the reference point with a genetic algorithm to find the Pareto Front in the solution space [41]. The basic procedure of NSGA-III is illustrated in Fig. 6.

In terms of the optimization problem in this paper, the detailed implementation steps are described in what follows.

Step 1) Individuals of each population are all composed of sixteen variables, namely PI parameters in Table I. The initial population is constituted by individuals formed by random principle within the allowable ranges.

Step 2) The twelve fitness values of the initial population are calculated by the combination of the small signal model in section II, fitness functions (10) and the data in the initial population.

Step 3) The population is classified into several fronts with the dominance theory and is sorted in ascending order. Besides, considering the constraint $\mathrm{Re}(\lambda_i) < 0$, it is specified that the individual with the smaller $\sum \mathrm{Re}(\lambda_i)$ has the higher rank.

Step 4) The optimization model normalizes the objectives, creates the reference points, associates each individual with a reference point, and computes niche count of reference points.

Step 5) In order to produce the new population which can maintain the superiority and diversity, the model applies the

tournament selection, the simulated binary crossover (SBX), and the polynomial mutation to the parent population.

Step 6) The steps 2, 3, and 4 are repeated to obtain fitness values, front ranks, and niche counts.

Step 7) According to the front ranks and niche counts, this step selects the appropriate individuals from the last population and the population constructed in step 5 to form the next population.

Step 8) Looping of steps 5, 6 and 7 are executed until the number of generation reaches the upper limit.

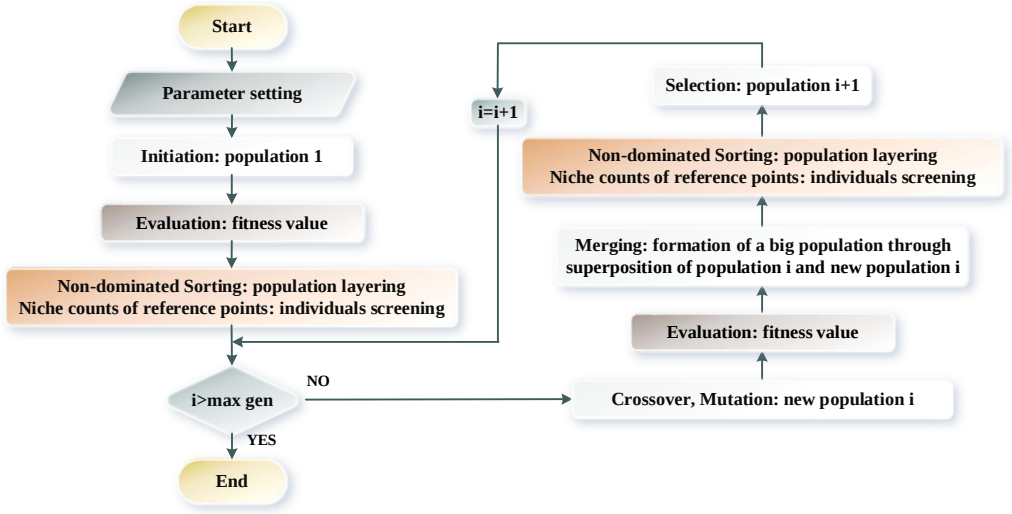

Fig. 6 Basic procedure of NSGA-III

B. t-SNE for Visual Analysis

Considering the developed optimization model, the objectives corresponding to the final solutions are high-dimensional, augmenting the difficulty to intuitively observe and evaluate the results of the algorithm. This paper employs the t-SNE method to reduce the dimension of the objectives. The core concept of t-SNE is to map data points in the high-dimensional space to low-dimensional space and maintain the spatial distance between data points unchanged, i.e., points that are close/far in high-dimensional space are still close/far in the low-dimensional space [42].

Suppose there is a dataset $X=\{x_1,\cdots,x_N\}$ in the high-dimensional space, and the conditional probability $p_{b|a}$ between x_a and x_b can be measured by Gaussian function:

$$p_{b|a}=\frac{\exp\left(-\left|x_a-x_b\right|^2/2\sigma_a^2\right)}{\sum_{k\neq a}\exp\left(-\left|x_a-x_k\right|^2/2\sigma_a^2\right)} \tag{11}$$

The similarity(distance) between x_a and x_b is defined as

$$X_{ab}=\left(p_{a|b}+p_{b|a}\right)/2N \tag{12}$$

Likewise, t-Distribution is used to calculate the similarity between low-dimensional mapping data points y_a and y_b:

$$Y_{ab} = \left(1+\left|y_a - y_b\right|^2\right)^{-1} \Big/ \sum_{k=1}\sum_{l\neq k}\left(1+\left|y_k - y_l\right|^2\right)^{-1} \tag{13}$$

Hence, a cost function that evaluates the relationship between data distribution in two different dimensions of space is given by the Kullback-Leibler (KL) divergence:

$$C = \sum_{a=1}\sum_{b=1,b\neq a} X_{ab} \ln\left(X_{ab}/Y_{ab}\right) \tag{14}$$

The optimal data points in low-dimensional space can be obtained by minimizing the cost function.

According to the analysis in section III, individuals of each generation contain twelve objectives. This paper uses t-SNE algorithm to visually analyze the individuals of each generation, as shown in Fig. 7. Considering the conclusion in section III that two modes $\lambda_{15,16}$ and $\lambda_{17,18}$ are strongly correlated with PI parameters, we can regard the number of essential characters of each individual as two. Then the Pareto front of each generation can be mapped into the two-dimensional plane, which underlies the intuitive observation of the development trend of objectives with the PI parameters variations. Moreover, the two-dimensional diagrams facilitate the generalization of PI parameters' optimal ranges.

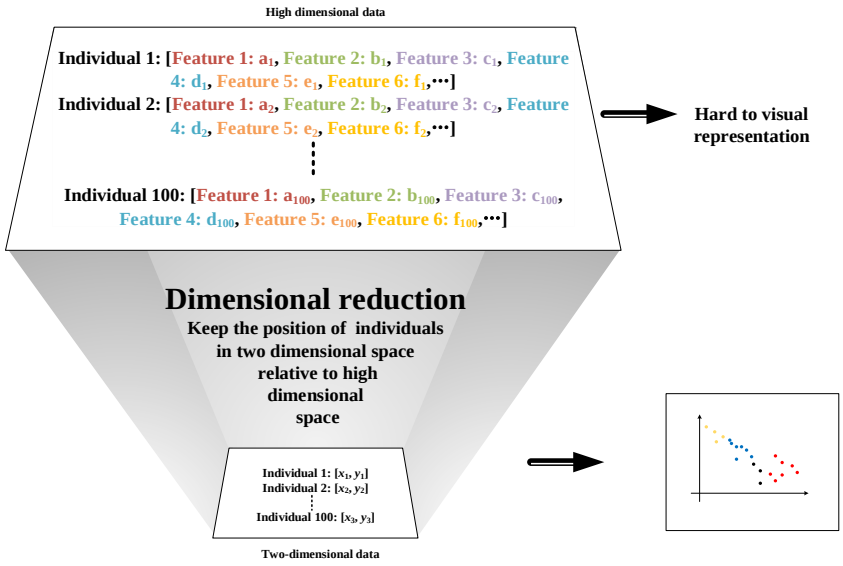

Fig. 7 Dimension reduction diagram

V. Results and Discussion

A. *Results of the Optimization Model*

The proposed optimization model is implemented on the MATLAB according to the process in Fig. 8. From the analysis results obtained for several model test cases, the following parameters of NSGA-3 were adopted:

- Population size is 200;
- Maximum number of generations is 100($ngen_{max}$);

- The crossover rate is 90%, the mutation rate is 50%, and the remaining individuals are obtained by recombination;
- Individuals differ in at least one gene.

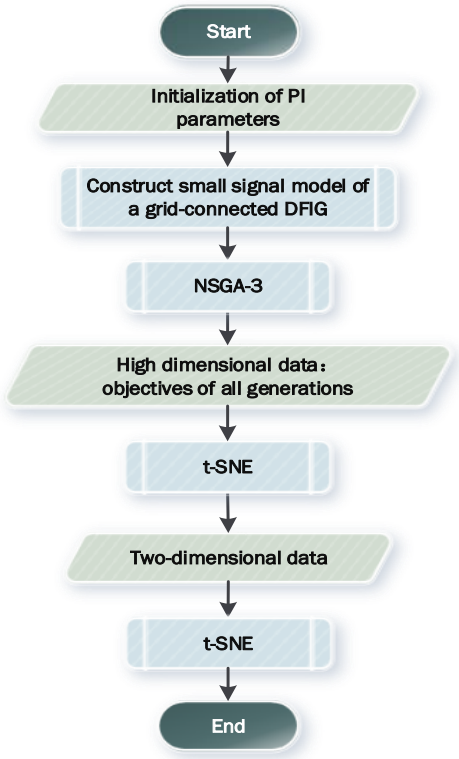

Fig. 8 Total flow of the optimization algorithm

After the dimension reduction with t-SNE, the Pareto fronts of the 1st generation and the 10th to 100th generations with the spacing of 10 generations are depicted in Fig. 9, where the colour bar represents the generation number. Fig. 9 illustrates that the mapping of the high-dimensional objects in low-dimensional space converges into several areas with the progress of optimization. Excluding some individual data, it can be found that objectives at the 100th generation marked with yellow circle gather together to form several yellow areas, which corresponds to the optimal ranges of PI parameters.

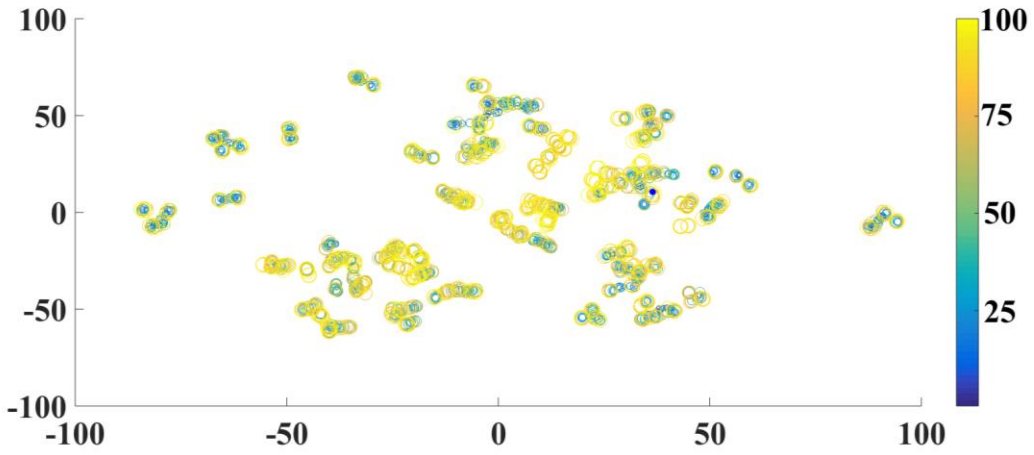

Fig. 9 Dimension reduction of Pareto fronts at 1st,10th, 20th, ⋯, 100th generation

Hence, except for individuals that deviate from the aggregated areas, PI parameters of individuals at the 100th generation's Pareto front form the optimal ranges of PI parameters, as shown in Fig. 10. The horizontal axis represents the PI parameters, and the values of PI parameters are transformed into per-unit values, where the base value of each PI parameter is its initial value in Table I. According to the Fig. 9 and 10, the optimal ranges of PI parameters are summarized in Table IV. Especially, K_{i4}, K_{i6}, and K_{i0} are scattered across the area, we regard to their original parameters as optimal parameters.

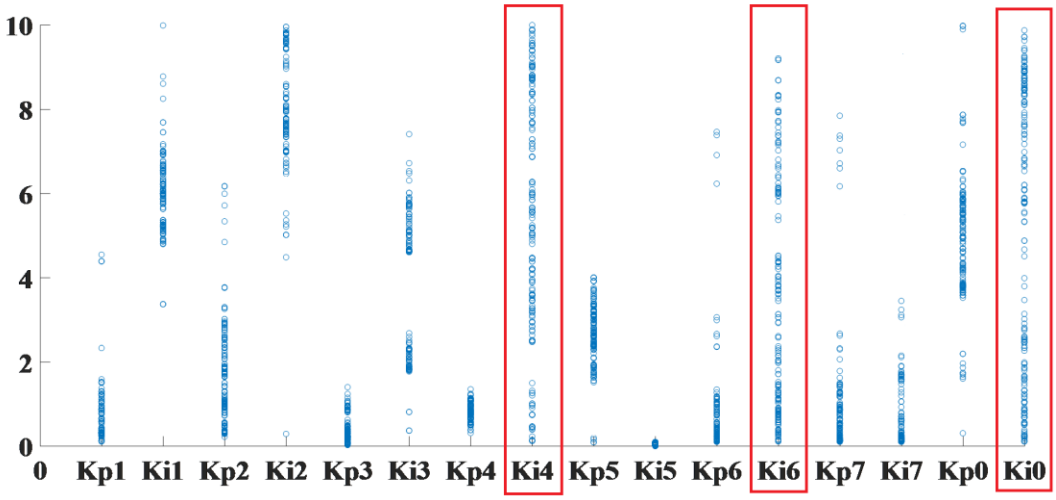

Fig. 10 Optimal range of PI parameters

Table IV OPTIMAL PI PARAMETERS

Symbol	Range	Symbol	Range
K_{p0}	950~1860	K_{i0}	1100
K_{p1}	0.005~0.05	K_{i1}	0.0018~0.0028
K_{p2}	0.5~15	K_{i2}	42~60
K_{p3}	0.05~0.5	K_{i3}	3×10^{-4}~5×10^{-4} or 9×10^{-4}~1.2×10^{-4}
K_{p4}	0.9~6	K_{i4}	5
K_{p5}	3.12~3.42	K_{i5}	6.5
K_{p6}	0.093~0.93	K_{i6}	0.05
K_{p7}	0.083~1.66	K_{i7}	2~38

B. The Stress Analysis of the Optimal PI Parameters

To study the stress of the optimal PI parameters, the traces of eigenvalues during the variation of the output power are investigated, as shown in Fig. 11. Based on the optimized controllers' PI parameters shown in Table IV, this paper increases the output power from 0.1 to 1 p.u. in the small signal model. The simulation results suggest that only $\lambda_{15,16}$, $\lambda_{17,18}$, and $\lambda_{19,20}$ change during the increase of the output power.

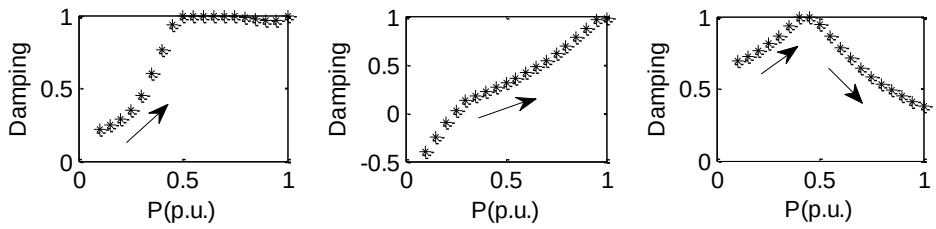

Fig. 11 Traces of eigenvalues as during the increase of generated power. (a) Traces of $\lambda_{15,16}$. (b) Traces of $\lambda_{17,18}$. (c) Traces of $\lambda_{19,20}$.

$\lambda_{15,16}$ are corresponding to SSCI oscillation mode. As shown in Fig. 11(a), the damping increases as the generated power increases, and it maintains to be 1 when the generated power is more than 0.5 p.u.. $\lambda_{17,18}$ are corresponding to SSO mode of the high-speed shaft. Fig. 11(b) suggests that the damping increases as the generated power increases. It should be emphasized that the damping is negative when the generated power is less than 0.24 p.u.. Therefore, the system is unstable and the controllers' parameters should be justified when the generated power is less than 0.24 p.u.. $\lambda_{19,20}$ are corresponding to low-frequency oscillation mode. Fig. 11(c) indicates that damping increases first and then decreases as the generated power increases. Hence, the optimal PI parameters have wide adaptability to the generated power, i.e., 0.24 to 1 p.u..

C. Time-domain Simulation Testing

In order to test the optimal PI parameters of the proposed optimization model, the system in Fig. 1 was implemented in Simulink. To compare the performance of SSCI, SSO, and low-frequency oscillations before and after the optimization, the parameters given in Tables I and IV are applied to the system separately. The FFT results of the dc-link voltage, the electromagnetic torque, and the rotor speed of the generator before and after parameters optimization are shown in Figs. 12-14.

Fig. 12 shows a comparison of the dynamic response of the dc-link voltage. It is observed from Fig. 12(a) that there exists oscillation at a frequency of 4.5 Hz corresponding to SSCI. Consequently, the 4.37 Hz oscillation frequency disappears in Fig. 12(b). Therefore, the system with optimized parameters shows superior performance for mitigating SSCI.

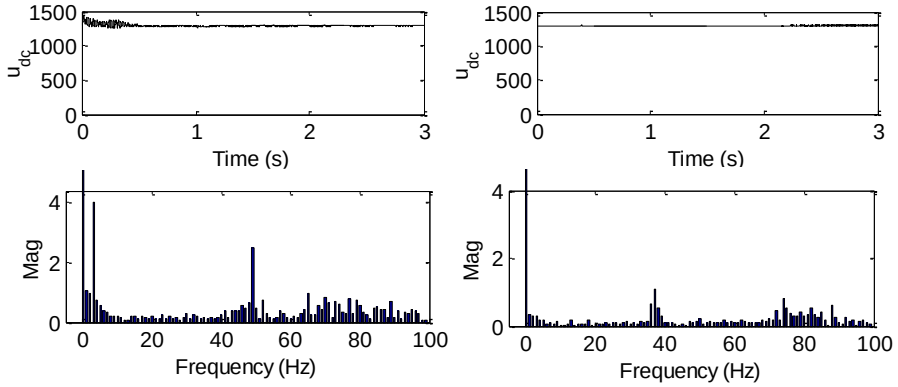

Fig. 12 FFT analysis of the dc-link voltage. (a) Before optimization. (b) After optimization.

Fig. 13 shows a comparison of the dynamic response of the electromagnetic torque T_e. Fig. 13(a) and (b) denote the system with original and optimized parameters. It is observed from Figs. 13(a) and (b) that there exist oscillations at frequencies of 2.5 Hz and 14 Hz, which are corresponding the SSO modes. It indicates that the system with optimized parameters can damp the vibrations quickly and effectively, and therefore, improves the damping of SSO.

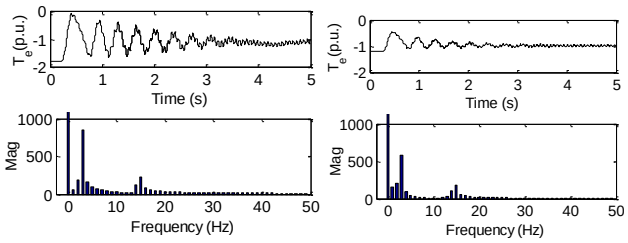

(a) (b)

Fig. 13 FFT analysis of the electromagnetic torque. (a) Before optimization. (b) After optimization.

Fig. 14 shows a comparison of the dynamic responses of the rotor speed of the generator. Fig. 14(a) and (b) denote the system with original and optimized parameters. It is observed from Figs. 14(a) and (b) that there exist harmonics Fig. 14(a) denotes the system with the original parameters and there exist harmonics at frequencies of 0.5 Hz corresponding to low-frequency oscillation, 2.5 Hz and 14 Hz corresponding to SSO. It indicates that the system with optimized parameters is able to damp the vibrations quickly and effectively, and therefore, improves the damping of low-frequency oscillation and SSO.

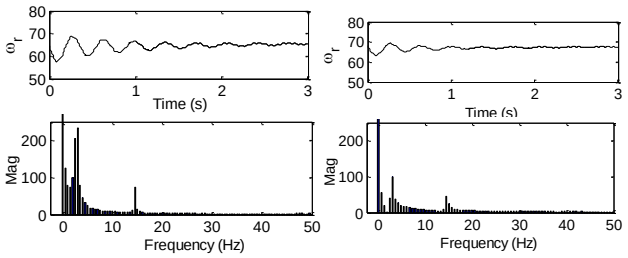

(a) (b)

Fig. 14 FFT analysis of the rotor speed of the generator. (a) Before optimization. (b) After optimization.

D. Practical Experiment Testing

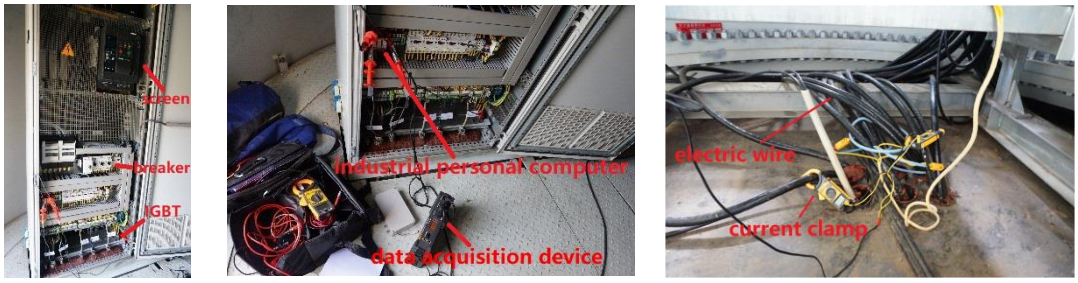

(a) (b) (c)

Fig. 15 Experimental photography in wind tower. (a) Converter cabinet. (b) Data acquisition device. (c) Current clamp.

For the sake of demonstration, this paper analyzes the monitoring data of a practical grid-connected DFIG which employs the optimal PI parameters. We monitor the data from converter cabinet in wind tower, as shown in Fig. 15. The sampling frequency of the data is 4000 Hz, the time-domain and frequency curve of output power are shown in Fig. 16. Because the DC component of the output power is too large to observe interactions, Fig. 17 provides the enlargement of several frequencies. The amplitude of the low-frequency oscillation, SSO and SSCI is around 2500, which is far less than the amplitude of the DC component. Thus, the

optimal PI parameters have an inhibitory effect on the interactions in the gird-connected DFIG system.

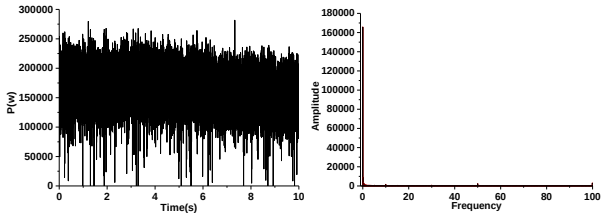

(a) (b)

Fig. 16 The FFT analysis results of the output active power of the wind turbine. (a) Time-domain signal. (b) Frequency domain signal.

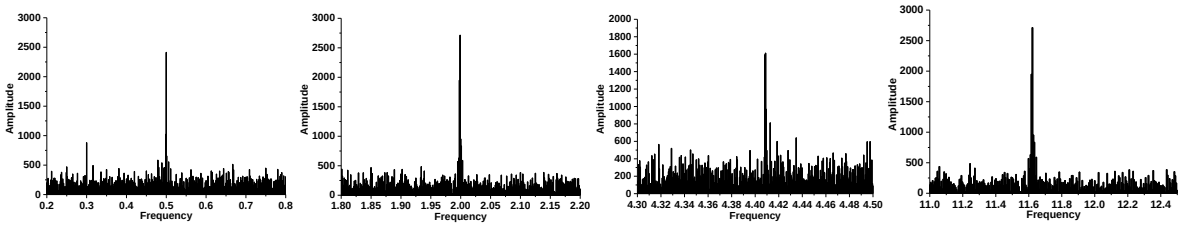

(a) (b) (c) (d)

Fig. 17 The enlarge of specific frequencies. (a) Low frequency oscillation(0.51 Hz). (b) SSO(2.0 Hz). (c) SSCI(4.37 Hz). (d) SSO(11.6 Hz).

For further validation, we analyze the output current of DFIG to capture vibrations of the system by Prony algorithm, as shown in Fig. 18 and Table V. Obviously, compared with No. 13, the amplitude of No. 2, 3, 4 and 7 is small, even less than one-tenth of No. 13, and the damping ratios of No. 2, 3, 4 and 7 are much bigger than No. 13. Hence, the proposed scheme is effective and practical to mitigate SSI existing in grid-connecter DFIG wind turbines.

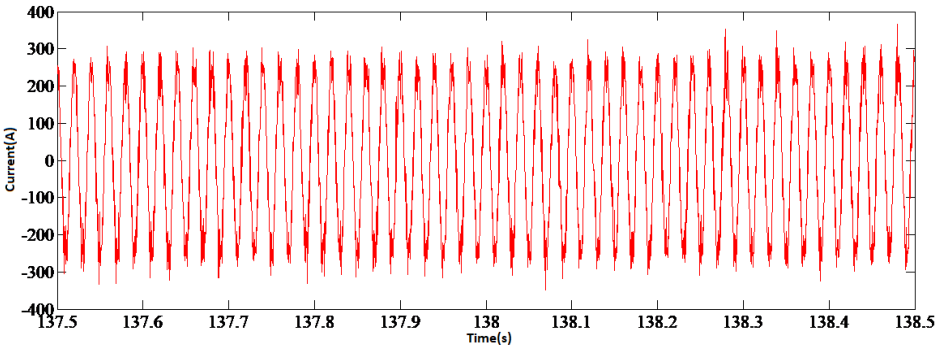

Fig. 18 The terminal output current of DFIG

Table V THE ANALYSIS RESULTS OF THE OUTPUT CURRENT BASED ON THE PRONY ALGORITHM

No.	Amplitude	Frequency/Hz	Damping ratio/%
1	12.4993	0.819(Low frequency)	29.280
2	8.9195	3.756（SSCI）	10.572
3	21.5360	5.499（SSCI）	13.573
4	10.2678	11.712（SSO）	13.575
5	21.2483	18.670	2.629
6	57.3626	24.224（SSR）	12.734
7	12.2640	24.748（SSR）	10.886
8	12.5002	32.079	1.353
9	12.6400	34.581	1.920
10	107.9499	40.009	8.849
11	38.3756	42.972	1.751

12	23.5963	44.256	0.793
13	220.2924	49.951	-0.087
14	38.1660	51.366	1.894
15	12.8859	53.223	0.913
16	19.1697	56.229	0.962
17	19.6096	57.855	0.690
18	24.1412	63.031	1.091
19	25.9850	65.039	0.648
20	44.3753	71.905	1.992

VI. CONCLUSION

The grid-connected DFIG wind turbines are prone to stability issues caused due to electric resonance, SSO, SSR, SSCI and low-frequency oscillation. The stability issues can be identified from small signal model eigenvalues and participation factors. A novel method is proposed herein to improve the stable region of DFIG by increasing the system damping with optimal PI parameters of converters. Simulation results validate the practicability and availability of the proposed method, thus extending lifespans of DFIG wind turbines. Moreover, Field data collected from an actual DFIG wind turbine is analyzed to check the effectiveness of the optimization model.

ACKNOWLEDGMENTS

This work is supported by the National Natural Science Foundation of China (51677114) and Research Program of State Grid Corporation of China (SGTYHT/16-JS-198). A. Chen thanks Miss C. Deng for her support in life and spirit.

APPENDIX

CORE PSEUDO CODE OF OPTIMIZATION METHOD(MATLAB)

Main function (Part A of Section V, Fig. 8)

pop.Indepvar: independent variables, i.e., PI parameters
pop.Cost: objectives
pop.Rank: rank of individuals at each generation
pop.Cons: constraints of individuals, i.e., pop.Cost < 0
nPop: individuals of each generation
pCrossover: probability of crossover
pMutation: probability of mutation
Maxgen: number of limited generations
popc: individuals after crossover
popm: individuals after mutation

```
Var = Value;                % initial parameters setting
for i = 1: nPop
PI_params = pop(i).Indepvar;
    Evaluation;
end
SortAndSelectPopulation;
nCrossover = 2*round(pCrossover*nPop/2);
nMutation = round(pMutation*nPop);
```

```
for it = 2:Maxgen
for k = 1:nCrossover/2
Crossover;
    end
    for k = 1:nMutation
Mutation;
    end
pop=[pop;popc;popm];
    for i = 1: N
        Evaluation;
    end
    SortAndSelectPopulation;
    save_data;
end
Visualize_data;
```

Evaluation (Section IV, calculation of (9) and (10))

DFIG_small_signal.mdl: Small-signal model of each part of grid-connected DFIG system is constructed in MATLAB/Simulink, and each model is connected with each other according to system's electrical diagram.(Section II)

```
[A,~,~,~] = linmod('DFIG_small_signal.mdl');
lambda = eig(A);
damp_ratio = -real(lambda)./sqrt(real(lambda).^2 + imag(lambda).^2);
pop(i).Obj=(-damp_ratio([8,9,12:21])).';
pop(i).Cons=sum(bsxfun(@times,bsxfun(@lt, -pop(i).Cost, 0.0), -pop(i).Cost));
```

Visualize_data (Part B of Section IV)

Total_Pareto: individuals' cost of 1^{st},10^{th},20^{th},...,100^{th} generation pareto front
parm: parameters of color and size
compute_mapping: a function in 'drtoolbox' toolbox

```
Total_Mapped_Data=compute_mapping(Total_Pareto,'tSNE',2,12);
figure(1);
scatter(Total_Mapped_Data(2:end,1),Total_Mapped_Data(2:end,2),parm,parm);
hold on;
scatter(Total_Mapped_Data(1,1),Total_Mapped_Data(1,2),[],'b','filled');
```

SortAndSelectPopulation: normal algorithm of non-dominated sorting and selection by reference points (Part A of Section IV, Fig. 6)

Crossover: normal algorithm (Part A of Section IV, Fig. 6)

Mutation: normal algorithm (Part A of Section IV, Fig. 6)

REFERENCES

[1] L. Bird, M. Bolinger, T. Gagliano, R. Wiser, M. Brown, and B. Parsons, "Policies and market factors driving wind power development in the United States," *Energy Policy*, vol. 33, pp. 1397-1407, July 2005.

[2] N. Hatziargyriou, and A. Zervos, "Wind power development in Europe," *Proceedings of the IEEE*, vol. 89, pp. 1765-1782, Dec. 2001.

[3] R. Pena, J. C. Clare, and G. M. Asher. "Doubly fed induction generator using back-to-back PWM converters and its application to variable-speed wind-energy generation," *IEEE Proceedings-Electric Power Applications*, vol. 143, pp. 231-241, May 1996.

[4] S. Müller, M. Deicke, and R. W. D. Doncker, "Doubly fed induction generator systems for wind turbines," *IEEE Industry Applications Magazine*, vol. 8, pp. 26-33, Aug. 2002.

[5] R. K. Patnaik, P. K. Dash, and K. Mahapatra, "Adaptive terminal sliding mode power control of DFIG based wind energy conversion system for stability enhancement," *International Transactions on Electrical Energy Systems*, vol. 26, pp. 750-782, June 2016.

[6] J. L. Domínguez-García, O. Gomis-Bellmunt, F. D. Bianchi, and A. Sumper, "Power oscillation damping supported by wind power: a review," *Renewable and Sustainable Energy Reviews*, vol. 16, pp. 4994-5006, Sep. 2012.

[7] D. H. R. Suriyaarachchi, U. D. Annakkage, C. Karawita, and D. A. Jacobson, "A procedure to study sub-synchronous interactions in wind integrated power systems," *IEEE Trans. Power Systems*, vol. 28, pp. 377-384, July 2012.

[8] M. R. A. Pahlavani, and H. A. Mohammadpour, "Damping of sub-synchronous resonance and low-frequency power oscillation in a series-compensated transmission line using gate-controlled series capacitor," *Electric Power Systems Research*, vol. 81, pp. 308-317, Feb. 2011.

[9] S. K. Salman, and A. L. Teo, "Windmill modelling consideration and factors influencing the stability of a grid-connected wind power-based embedded generator," *IEEE Trans. Power Systems*, vol. 18, pp. 793-802, Mar. 2004.

[10] S. M., Muyeen, M. Hasanali, RionTakahashi, et al, "Transient stability analysis of grid connected wind turbine generator system considering multi-mass shaft modelling," *Electric Power Components and Systems*, vol. 34, pp. 1121-1138, Feb. 2006.

[11] IEEE Subsynchronous Resonance Working Group, "Terms, definitions and symbols for subsynchronous oscillations," *IEEE Trans. Power Apparatus and Systems*, vol. 104, pp. 1326-1334, June 1985.

[12] H. D. Battista, P. F. Puleston, R. J. Mantz, and C. F. Christiansen, "Sliding mode control of wind energy systems with DOIG-power efficiency and torsional dynamics optimization," *IEEE Trans. Power Systems*, vol. 15, pp. 728-734, May 2000.

[13] F. D. Bianchi, D. H. Battista, and R. J. Mantz, *Wind turbine control systems: principles, modelling and gain scheduling design*, Springer Science & Business Media, 2006.

[14] J. F. Manwell, J. G. McGowan, and A. L. Rogers, *Wind energy explained: theory, design and application*. John Wiley & Sons, 2010.

[15] IEEE Subsynchronous Resonance Working Group, "Reader's guide to subsynchronous resonance," *IEEE Trans. Power Syst*, vol. 7, pp. 150-157, Feb. 1992.

[16] M. S. El-Moursi, B. Bak-Jensen, and M. H. Abdel-Rahman, "Novel STATCOM controller for mitigating SSR and damping power system oscillations in a series compensated wind park," *IEEE Trans. Power Electronics*, vol. 25, pp. 429-441, Aug. 2009.

[17] L. Fan, and Z. Miao, "Mitigating SSR using DFIG-based wind generation," *IEEE Trans. Sustainable Energy*, vol. 3, pp. 349-358, July 2012.

[18] F. D. Jesus, E. H. Watanabe, L. F. W. D. Souza, and J. E. R. Alves, "SSR and power oscillation damping using gate-controlled series capacitors (GCSC)," *IEEE Trans. Power Delivery*, vol. 22, pp. 1806-1812, July 2007.

[19] R. K. Varma, S. Auddy, and Y. Semsedini, "Mitigation of subsynchronous resonance in a series-compensated wind farm using FACTS controllers," *IEEE Trans. Power Delivery*, vol. 23, pp. 1645-1654, June 2008.

[20] A. Ostadi, A. Yazdani, and R. K. Varma, "Modelling and stability analysis of a DFIG-based wind-power generator interfaced with a series-compensated line," *IEEE Trans. Power Delivery*, vol. 24, pp. 1504-1514, June 2009.

[21] L. C. Gross, "Sub-synchronous grid conditions: New event, new problem, and new solutions," *37th Annual Western Protective Relay Conference, Spokane, Washington*. 2010.

[22] G. D. Irwin, "Sub-synchronous interactions with wind turbines," *Technical Conference-CREZ System Design and Operation*, 2010.

[23] NERC LL-45 Lesson Learned – "Sub-Synchronous Interaction between Series-Compensated Transmission Lines and Generation," July 26, 2011.

[24] R. Nath, and C. G. Moran, "Study of sub-synchronous control interaction due to the interconnection of wind farms to a series compensated transmission system," *Transmission and Distribution Conference and Exposition (T&D),* May 2012.

[25] G. D. Irwin, K. J. Amit, and A. L. Isaacs, "Sub-synchronous control interactions between type 3 wind turbines and series compensated AC transmission systems," *Power and Energy Society General Meeting,* July 2011.

[26] E. V. Larsen, and D. A. Swann, "Applying power system stabilizers part ii: Performance objectives and tuning concepts," *IEEE Trans. Power Apparatus and Systems*, vol. 6, pp. 3025-3033, June 1981.

[27] J. Ma, P. Zhang, H. J. Fu, B. Bo, and Z. Y. Dong, "Application of phasor measurement unit on locating disturbance source for low-frequency oscillation," *IEEE Trans. Smart Grid*, vol. 1, pp. 340-346, Dec. 2010.

[28] W. Kao, "The effect of load models on unstable low-frequency oscillation damping in Taipower system experience w/wo power system stabilizers," *IEEE Trans. Power Systems*, vol. 16, pp. 463-472, July 2001.

[29] Y. Zhang, D. Xie, J. Feng, and R. Wang, "Small-signal Modelling and Modal Analysis of Wind Turbine Based on Three-mass Shaft Model," *Electric Power Components and Systems*, vol. 42, pp. 693-702, Apr. 2014.

[30] A. Tabesh, and R. Iravani, "Small-signal dynamic model and analysis of a fixed-speed wind farm-a frequency response approach," *IEEE Trans. Power Delivery*, vol. 21, pp. 778-787, Mar. 2006.

[31] H. Huang, C. Mao, et al, "Small-signal modelling and analysis of wind turbine with direct drive permanent magnet synchronous generator connected to power grid," *IET Renewable Power Generation*, vol. 6, pp. 48-58, Jan. 2012.

[32] Y. Mishra, S. Mishra, et al. "Small-signal stability analysis of a DFIG-based wind power system under different modes of operation," *IEEE Trans. Energy Conversion*, vol. 24, pp. 972-982, Nov. 2009.

[33] H. Liu, X. Xie, J. He, et al, "Subsynchronous Interaction between Direct-Drive PMSG Based Wind Farms and Weak AC Networks," IEEE Transactions on Power Systems, vol. 32, pp. 4708-4720, Mar. 2017.

[34] A. E. Leon, "Integration of DFIG-Based Wind Farms Into Series-Compensated Transmission Systems," IEEE Transactions on Sustainable Energy, vol. 7, pp. 451-460, April 2016.

[35] M. Ghafouri, U. Karaagac, H. Karimi, S. Jensen, J. Mahseredjian, & S. O. U. Faried, "An LQR Controller for Damping of Subsynchronous Interaction in DFIG-Based Wind Farms," IEEE Transactions on Power Systems, vol. 32, pp. 4934-4942, Feb. 2017.

[36] H. Mohammadpour and E. Santi, “Modeling and control of gatecontrolled series capacitor interfaced with a DFIG-based wind farm,” IEEE Transactions on Industrial Electronics, vol. 62, pp. 1022–1033, Feb. 2015.

[37] M. Darabian, and A. Jalilvand, "Improving power system stability in the presence of wind farms using STATCOM and predictive control strategy," IET Renewable Power Generation, vol. 12 pp. 98-111, Jan. 2018.

[38] Y. Wang, Q. Wu, and S. Kang, "Sub-synchronous interaction analysis between DFIG based wind farm and series compensated network," IEEE PES Asia-Pacific Power and Energy Engineering Conference (APPEEC), Oct. 2016.

[39] F. Fateh, W. N. White, and D. Gruenbacher, “Torsional vibrations mitigation in the drivetrain of DFIG-based grid-connected wind turbine” *IEEE Trans. Industry Applications*, vol. 53, pp. 5760-5767, Nov.-Dec. 2017.

[40] G. Mandic, A. Nasiri, E. Muljadi, and F. Oyague, "Active Torque Control for Gearbox Load Reduction in a Variable Speed Wind Turbine," *IEEE Trans. Industrial Electronics*, vol. 48, pp. 2424-2432, Nov.-Dec. 2012.

[41] H. Jain, and K. Deb, "An Evolutionary Many-Objective Optimization Algorithm Using Reference-Point Based Nondominated Sorting Approach, Part II: Handling Constraints and Extending to an Adaptive Approach," *IEEE Trans. Evolutionary Computation*, vol. 18, pp. 602-622, Aug. 2014.

[42] N. Pezzotti, B. P. F. Lelieveldt, L. V. D. Maaten, T. Hollt, E. Eisemann, and A. Vilanaova, "Approximated and User Steerable tSNE for Progressive Visual Analytics," *IEEE Trans. Vis Comput Graph*, vol. 23, pp. 1739-1752, May 2016.